Localized plasmon resonance in boron-doped multiwalled carbon nanotubes

M. V. Shuba,[1,2] D. I. Yuko,[1] P. P. Kuzhir,[1,2] S. A. Maksimenko,[1,2] G. G. Chigir,[3] A. N. Pyatlitski,[3] O. V. Sedelnikova,[2,4] A. V. Okotrub,[2,4] and Ph. Lambin[5]

[1]*Institute for Nuclear Problems, Belarusian State University, Bobruiskaya 11, 220050 Minsk, Belarus*

[2]*Tomsk State University, Lenin Avenue 36, 634050, Tomsk, Russia*

[3]*Open Joint Stock Society INTEGRAL—INTEGRAL Holding Managing Company, Kazintsa I.P. Str., 121A, 220108 Minsk, Belarus*

[4]*Nikolaev Institute of Inorganic Chemistry, SB RAS, 3 Acad. Lavrentiev Av., 630090 Novosibirsk, Russia*

[5]*Physics Department, Université de Namur, 61 Rue de Bruxelles, B-5000 Namur, Belgium*

(Received 22 February 2018; published 16 May 2018)

Substitutionally boron-doped multiwalled carbon nanotubes (B-CNTs) with lengths mainly less than 0.5 μm and diameters 10–30 nm have been obtained by arc-discharge evaporation of the graphite anode containing boron material. The broad peak has been observed in the midinfrared conductivity spectra of the thin film comprising B-CNTs. The peak was suggested to be associated with a phenomenon known as localized plasmon resonance. Theoretical analysis has been done to confirm the possibility of this phenomenon to occur in the B-CNTs.

DOI: 10.1103/PhysRevB.97.205427

I. INTRODUCTION

A localized plasmon resonance (LPR) occurs due to the confinement of a surface plasmon wave. The LPR in carbon nanostructures has been actively studied in recent years with respect to its application in the terahertz and midinfrared plasmonics [1]. Different structures with LPR have been investigated, including single-layer or bilayer graphene-nanodiscs [2,3], graphene nanoribons [1], graphene-coated nanospheres [4], single- [5–9], and multiwalled [10,11] carbon nanotubes (CNTs). The doping was found to be a very effective way to change the conductivity of carbon nanoparticles and tune the LPR frequency [1,6]. In spite of the great interest in the plasmonic effect in carbon nanostructures, the LPR in doped multiwalled CNTs (MWNTs) has not been investigated yet.

Optical properties of single-walled CNT (SWNT)-based films have been intensively studied for the past two decades [7,12–14]. The absorbance of the SWNT films in the midinfrared range (≈12–120 THz) is the result of both the intra- and interband electron transitions. CNT films have absorbance bands [15] in the range 100–270 THz due to the first interband electron transitions in the semiconducting SWNTs with a diameter of 1–2 nm. The LPR in finite-length metallic or doped semiconducting SWNTs leads to a broad terahertz peak in the conductivity spectra of the CNT films [7,12,13]. The LPR frequency f_p depends on the tube length [5,7]; typically f_p is in the range 3–30 THz for a CNT length of 0.1–1 μm. Since the surface wave velocity in the bundle of SWNTs is higher than in individual tubes, the LPR phenomena in SWNT bundles occurs at higher frequencies; e.g., $f_p \approx 45$ THz for a bundle comprising only metallic SWNTs and having a length of 500 nm and diameter of 54 nm [16]. To obtain the LPR in the midinfrared range, one needs to have all the SWNTs in the bundle be metallic or heavily doped semiconducting (i.e., doping-induced shift of chemical potential should be large enough to produce a sizable electron or hole charge density [17]).

Resonant behavior of MWNT-based film has been observed in the terahertz [11], but not in the midinfrared range. The main reason is that a large number of interband transitions in different shells of MWNT acting simultaneously produce monotonic frequency dependence of the tube conductance Σ in visible and infrared ranges [10]. Due to the inequality, $\mathrm{Re}\,\Sigma > \mathrm{Im}\,\Sigma$, the surface plasmon is strongly attenuated in MWNTs and, consequently, the LPR does not occur [10].

To suppress interband transitions and increase the number of intraband transitions, one can use substitutional doping of CNTs. Relatively weak doping (<2 at.%) with nitrogen (N) or boron (B) atoms practically does not modify the electronic band structure, but results in a Fermi-level shift of up to 1 eV [6,18–21]. The shift of the Fermi energy to the conduction or valence band, for N or B doping, respectively, leads to the opening of additional conducting channels for the charge carriers. The number of open channels is determined by the number of electronic sub-bands crossing the Fermi level. Simultaneously, doping leads to the suppression of the interband transitions from these sub-bands. Then, the condition of the surface wave propagation, $\mathrm{Re}\,\Sigma < \mathrm{Im}\,\Sigma$, becomes true and the LPR is expected to be observed in doped MWNTs in the midinfrared range. Since the electronic band gap is narrow (<0.15 eV) for shells of large diameter (>6 nm), relatively weak doping (Fermi shift ≈0.1 eV) can provide conditions required for the LPR phenomena in MWNTs.

In the present paper, we report the observation of the midinfrared LPR in films comprising B-doped MWNTs produced by arc-discharge method. The calculation of the absorption cross-section of finite-length doped CNTs confirm the possibility of the LPR in the midinfrared regime.

II. EXPERIMENTAL RESULTS

The study of B- and N-doped MWNTs is presented in detail in the reviews [22,23]. The morphology of doped

MWNTs depends strongly on the fabrication method [22]. CNTs synthesized with chemical vapor deposition approach are very defective, containing seriously curved, waved, or buckled graphene layers [24,25]. MWNTs obtained with arc-discharge method are straight and have more perfect crystalline structure [26,27]. Moreover, their length could be less than 1 μm [27], which is preferable for the observation of the LPR phenomenon in the midinfrared range. Modified arc-discharge method with 15 wt.% boron packed into the anode was used to obtain MWNTs with 0.7 at.% boron incorporated into the CNT lattice [26]. It was sufficient to form a p-type semiconductor.

In our study, we used B-doped MWNT material (referred to here as B-CNTs) synthesized in a setup for electric-arc graphite evaporation [28]. The electric-arc discharge was maintained at a current of 500 A and voltage of 40 V. The cathode made of graphite was 60 mm in diameter. The anode was a graphite rod 14 × 14 mm in cross-section and 200 mm long. A hole, 10 mm in diameter, was drilled at the anode center and filled with amorphous boron (10 wt.%). Helium at a pressure of 750 Torr was used as a buffer gas. Evaporation of the anode material resulted in the formation of a dense carbon deposit on the cathode. Undoped pristine MWNT material was also obtained by evaporation of a pure graphite rod [29].

Details of B-CNT characterization are presented in Ref. [27]. Briefly, both transmission electron microscopy and near-edge x-ray absorption fine structure spectroscopy indicated that the walls of synthesized B-CNTs are well graphitized [27]. X-ray photoelectron spectroscopy showed the presence of carbon (94%), oxygen (5%), and boron (1%) on the sample surface [27]. Additionally, about 70% of boron atoms were embedded in the graphite lattice of MWNTs, whereas about 30% of boron atoms were in the composition of B_2O_3 as impurities. Many onionlike spherical or polyhedral structures (multishell fullerenes) are formed in the sample [29].

Both pure- and doped-CNT films, with thickness of $\approx$1 μm, were fabricated via the vacuum filtration technique [30,31]. A typical scanning electron microscopy (SEM) image of the B-CNT film is represented in Fig. 1(a). One can see that tubes are straight and their lengths do not exceed 1 μm. Length distribution is shown in Fig. 1(b). There are many quasispherical particles; their fraction was estimated to be less than 30%.

Static electrical conductivity of thin films was measured at room temperature using a four-point linear probe method. The conductivity of the films comprising undoped CNTs and B-CNTs was 120 and 420 S/m, respectively.

Transmittance spectra of the CNT films were obtained at normal incidence using a time-domain terahertz spectrometer (0.1–2 THz, EKSPLA, Lithuania), a Fourier-transform infrared spectrometer Vertex 70 (2–270 THz, Bruker), and an RV2201 spectrophotometer (270–1000 THz, ZAO SOLAR, Belarus). The conductivity spectra of the films was calculated from the transmittance spectra via the Kramer-Kronig relation [8].

Figure 2 represents the frequency dependence of the optical density (OD) and the real part of the effective conductivity for undoped and B-doped CNT films. As shown in Fig. 2, both OD and Re(σ_{eff}) are monotonic for undoped tubes, whereas they have a broad peak in the midinfrared range for doped ones. The peak frequency in the OD and conductivity spectra

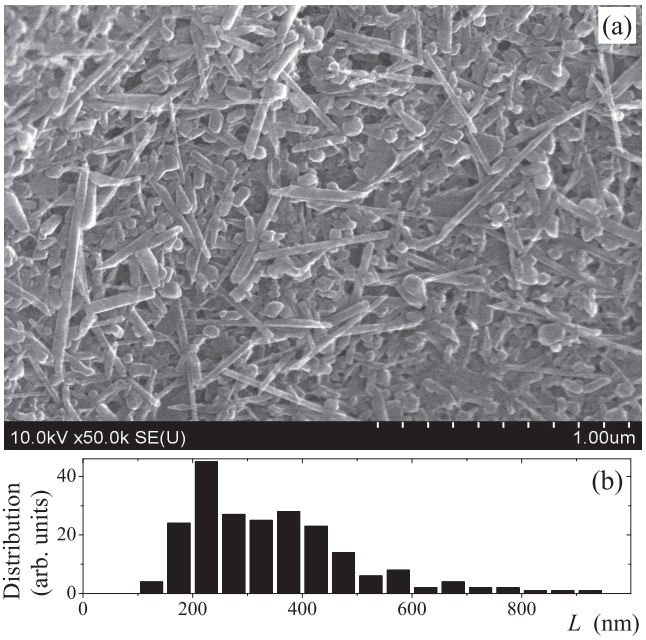

FIG. 1. (a) SEM image of the film comprising B-doped CNTs. (b) Length distribution obtained from SEM images of B-doped CNTs.

is 120 and 60 THz, respectively. The difference in the peak positions in Figs. 2(a) and 2(b) is due to the strong increase of the background OD with frequency. We can say that some resonance phenomenon takes place at about 60 THz.

To confirm that the peak is caused by MWNTs but not other different carbon nanoparticles present in the samples, we synthesized carbon material by the electric-arc discharge method at a current of 800 A and voltage of 45 V. The obtained sample contained a small fraction (<1 at.%) of MWNTs and had no peak in the midinfrared conductivity spectra.

It should be noticed that the theoretical analysis of the electronic properties of highly N- or B-doped SWNTs predicted midinfrared absorption peak in the range 70–120 THz

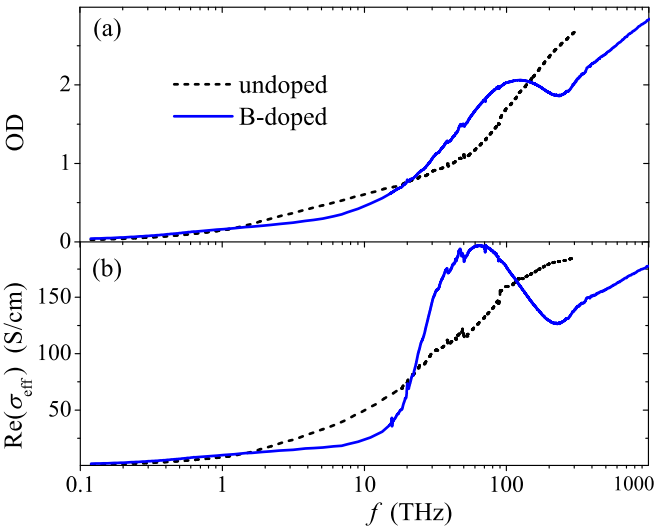

FIG. 2. (a) Optical density and (b) conductivity spectra of the films comprising undoped and B-doped CNTs.

[23,32,33]. This peak was observed for 15 at.% B doped SWNTs and associated with the interband transitions in the defective single-walled BC_3 nanotubes [32].

Our samples do not contain SWNTs and the doping is much lower (<1 at.%). We suppose that the peak we observed may be associated with the LPR phenomenon in doped MWNTs. The LPR occurs when tube length L equals a half wavelength $\lambda_s/2$ of the surface wave in MWNTs. According to Fig. 1(b), the average tube length in the sample is ≈300 nm, then $\lambda_s = 2L \approx 600$ nm at a frequency of 60 THz. This means that the surface wave in the doped MWNTs is slowed down having a phase velocity about eight times less than the speed of light in vacuum.

To confirm the possibility of the LPR phenomenon in doped MWNTs, in the next section, we propose a theoretical analysis of the midinfrared response of individual nanotubes and CNT film.

III. THEORETICAL RESULTS AND DISCUSSION

Ab initio quantum-mechanical simulations of substitutionally doped SWNTs show a shift of the Fermi level down to the valence band by 0.5–1 eV at 1–2 at.% B doping [20,21]. In our theoretical analysis, we shall describe the doping effect by the chemical potential μ defined as the Fermi-level shift; in undoped CNTs, $\mu = 0$.

Let the MWNT consist of N shells. The pth shell, $p = 1,2,...N$, has cross-sectional radius R_p, $R_N < R_{N-1} < ... < R_1$. We shall model a doped MWNT as a finite-length multishell structure composed of coaxial, infinitesimally thin conductive cylinders. The axial surface conductivity of the pth shell, denoted by σ_p, is considered to be the same as the conductivity of a doped SWNT with the same geometrical parameters and electron relaxation time $\tau = 10$ fs [34]. Assuming adjacent shells to be incommensurate, we shall neglect electron tunneling between the shells. Based on the quantum transport theory in the tight-binding approximation used for σ_p (see supplementary material in Ref. [14]), we computed the axial surface conductance $\Sigma_p = 2\pi R_p \sigma_p$ of the doped shell of a MWNT versus its diameter $2R_p$.

Figure 3 shows the dependence of the values $\mathrm{Re}(\Sigma_p)$ and $\mathrm{Im}(\Sigma_p)$ on the shell diameter at different chemical potentials μ. One can see two tendencies: (i) the conductance increases with shell diameter and (ii) the larger the chemical potential, the stronger the dependence of the conductance on the diameter. If the values of μ and R_p for doped tubes ($\mu > 0$) increase, the number of the crossings between electron sub-bands and Fermi level increases, and, consequently, the contribution of the intraband transitions to the shell conductivity increases as well. Simultaneously, the contribution of interband transitions to Σ decreases. As a result, inequality, $\mathrm{Re}(\Sigma_p) < \mathrm{Im}(\Sigma_p)$, becomes true for all the doped shells $p \in \{1,2..N\}$, and low attenuated surface waves can propagate along doped MWNTs, leading to the LPR phenomenon. Moreover, energy dissipation is lower for tubes with larger chemical potentials μ. Thus, doping leads to the "metallization" of the semiconducting shells, significantly increasing the imaginary part of their conductance over the real one.

The conductivity of undoped shells vs diameter displays sharp oscillations ($\mu = 0$ eV in Fig. 3) due to the transfer from

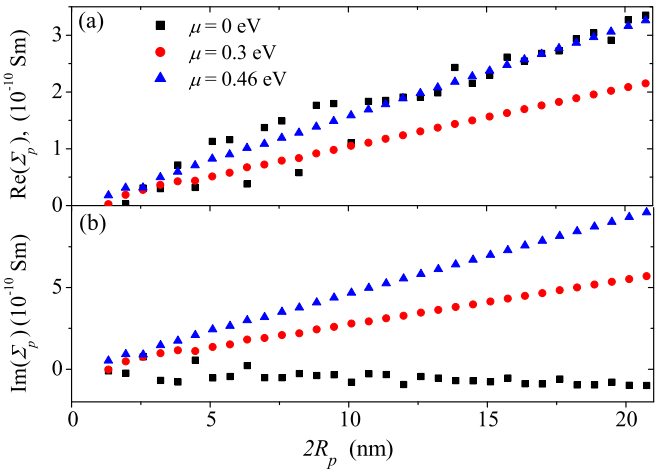

FIG. 3. (a) The real and (b) imaginary parts of the pth shell conductance Σ_p versus shell diameter $2R_p$ at frequency 50 THz, temperature 300 K, and different chemical potentials $\mu = 0$, 0.3, and 0.46 eV. The pth shell has chiral indexes $(261 - 8p,0)$.

semiconducting to metallic types of the conductivity and vice versa when chiral indices of the shells change. Let us notice that inequality $\mathrm{Re}(\Sigma_p) > \mathrm{Im}(\Sigma_p)$ for undoped shells leads to a strong attenuation of the surface wave in the MWNT, hindering the LPR phenomenon [10].

Let B-doped CNT be exposed to an externally incident field with frequency f and aligned parallel to the tube axis. To show the LPR in doped MWNTs, we calculated the normalized absorption cross section $\Lambda = 4\pi f \mathrm{Im}(\alpha)/(cR_1L)$ of MWNT with length L, and outer diameter $2R_1$. The polarizability α of the MWNT was computed using the integral equation technique applied to a boundary value problem for a system of finite-length coaxial impedance cylinders [35]. CNT contained $N = 14$ shells. The pth shell, $p = 1,2...N$, had chiral indices $(137 - 8p,0)$, $(269 - 8p,0)$, and $(392 - 8p,0)$ for tubes with outer diameters of ≈10, 20, and 30 nm, respectively. The axial surface conductivity of each shell was calculated at temperature 300 K and electron relaxation time of 10 fs in the same way as for Fig. 3.

Figures 4(a)–4(c) show the frequency dependence of Λ at different chemical potentials μ, lengths L, and diameters D of MWNTs. One can see from Fig. 4(a) that the spectrum for undoped MWNT ($\mu = 0$ eV) is monotonic, whereas the spectra for doped MWNTs have a peak due to LPR. The LPR frequency increases as tube length decreases or tube diameter increases [see Figs. 4(b) and 4(c)]. The LPR peak is more intensive and its frequency is higher for heavier doped MWNTs.

To calculate the effective permittivity of the MWNT-based film, we applied an adapted Waterman-Truell formula [36]

$$\varepsilon_{\mathrm{eff}}(f) = 1 + \frac{1}{3\epsilon_0} \sum_m \int_0^\infty \alpha_m(f,L) N_m(L) dL\,, \qquad (1)$$

where $\varepsilon_0 = 8.85 \times 10^{-12}$ Fm^{-1}; the function $N_m(L)$ describes the number density of the CNTs of type m with outer radius R_m, length L, and polarizability $\alpha_m(f,L)$. We defined the volume fraction of CNTs in the film as $\sum_m \int_0^\infty \pi R_m^2 L N_m(L) dL$. The factor 1/3 in Eq. (1) is due to the random orientations of the

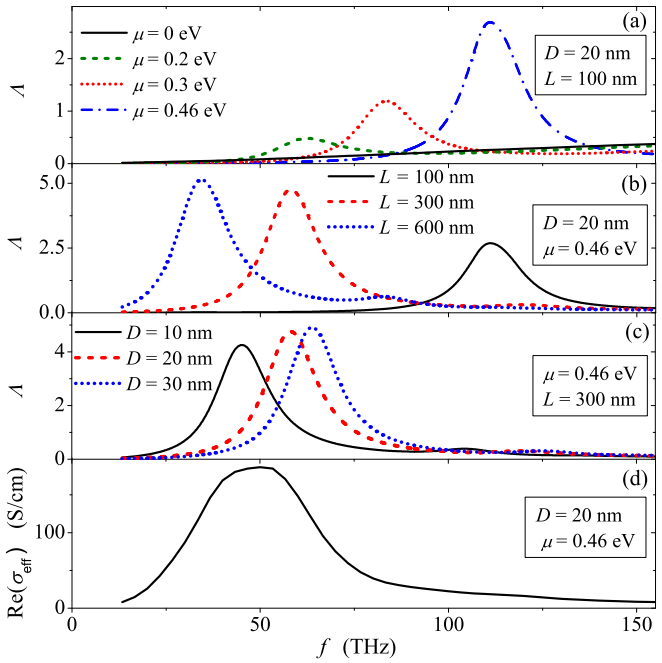

FIG. 4. Frequency dependence of the normalized absorption cross section Λ of the CNT at different (a) chemical potentials $\mu \in \{0,0.2,0.3,0.46\}$eV, $L = 100$ nm, $D = 20$ nm, (b) tube lengths $L \in \{100,300,600\}$ nm, $\mu = 0.46$ eV, $D = 20$ nm, and (c) outer diameters $D \in \{10,20,30\}$ nm, $\mu = 0.46$ eV, $L = 300$ nm. (d) The conductivity spectrum of the film comprising identically B-doped CNTs with diameter of 20 nm and length distribution as in Fig. 1(b); CNT volume fraction is 20%, $N = 14$ and $\mu = 0.46$ eV.

CNTs. The effective conductivity of the film can be found as follows: $\sigma_{\text{eff}} = 2\pi f \varepsilon_0(\varepsilon_{\text{eff}} - 1)$.

Figure 4(d) shows the frequency dependence of $\text{Re}[\sigma_{\text{eff}}]$ for the film, comprising identically B-doped CNTs with identical outer diameters $D = 20$ nm and numbers of shells $N = 14$ at tube volume fraction of 20%, and length distribution the same as in the experimental samples [see Fig. 1(b)]. As shown in Fig. 4(d), the conductivity spectrum has a broad peak at 50 THz due to the LPR phenomenon in the doped CNTs. In our experiment, we observed a broad conductivity peak in the same frequency range [see Fig. 2(b)]. This supports our suggestion that the physical mechanism of the observed midinfrared peak could be associated with the LPR in the B-doped MWNTs. The frequency of the observed LPR is two times higher than that reported for short-length SWNTs [7]; it can be tuned in a wide range (20–120 THz) by variation of diameter, length, and chemical potential of the MWNTs.

Let us note that the measured spectrum for B-CNTs in Fig. 2(b) beyond the LPR peak has an increase of conductivity with frequency in the range 10–1000 THz. This may be (i) a result of interband transitions in thin MWNTs ($D <$ 10 nm), in which weak doping cannot provide "metallization" of small-diameter shells, and (ii) a "tail" of π plasmon, which occurs at 5.5–6.0 eV in multishell fullerenes and MWNTs [37]. Since our theoretical analysis is carried out only for thick B-doped MWNTs, it cannot describe the behavior of conductivity beyond the midinfrared peak.

IV. CONCLUSION

Arc-discharge method has been applied to synthesize multiwalled CNTs substitutionally doped by less than 1 at.% boron. B-doped CNTs have the average length of ≈300 nm and diameter of 10–30 nm. Thin films comprising these tubes demonstrated a broad peak at 40–60 THz in the conductivity spectra. The peak was suggested to be associated with the LPR phenomenon. The doping was supposed to shift the Fermi level, changing CNT conductivity, and providing the condition required for surface wave propagation in the CNTs. As a result, the LPR in doped MWNTs could be observed in the midinfrared range. Theoretical analysis confirmed the possibility of the LPR phenomenon in the range 20–120 THz for the MWNTs with length <500 nm, outer diameter 10–30 nm, and chemical potential 0.2–0.5 eV.

ACKNOWLEDGMENTS

This research was partially supported by the Belarusian Republican Foundation for Fundamental Research (BRFFR) under Projects No. F18Kor-002 and No. F17RM-068, and Russian Foundation for Basic Research (No. 17-52-04077), as well as by the H2020-MSCA-RISE-2014 Project No. 644076 CoExAN, and H2020 RISE 734164 Graphene 3D. M.V.S., P.P.K., S.A.M., O.V.S., and A.V.O. are thankful for support by Tomsk State University Competitiveness Improvement Program.

[1] T. Low and P. Avouris, ACS Nano **8**, 1086 (2014).
[2] F. H. L. Koppens, D. E. Chang, and F. J. G. de Abajo, Nano Lett. **11**, 3370 (2011).
[3] W. Wang, S. Xiao, and N. A. Mortensen, Phys. Rev. B **93**, 165407 (2016).
[4] T. Christensen, A.-P. Jauho, M. Wubs, and N. A. Mortensen, Phys. Rev. B **91**, 125414 (2015).
[5] M. V. Shuba, G. Y. Slepyan, S. A. Maksimenko, and G. W. Hanson, J. Appl. Phys. **108**, 114302 (2010).
[6] A. M. Nemilentsau, M. V. Shuba, G. Y. Slepyan, P. P. Kuzhir, S. A. Maksimenko, P. N. D'yachkov, and A. Lakhtakia, Phys. Rev. B **82**, 235424 (2010).
[7] M. V. Shuba, A. G. Paddubskaya, A. O. Plyushch, P. P. Kuzhir, G. Y. Slepyan, S. A. Maksimenko, V. K. Ksenevich, P. Buka, D. Seliuta, I. Kasalynas, J. Macutkevic, G. Valusis, C. Thomsen, and A. Lakhtakia, Phys. Rev. B **85**, 165435 (2012).
[8] Q. Zhang, E. H. Haroz, Z. Jin, L. Ren, X. Wang, R. S. Arvidson, A. Luttge, and J. Kono, Nano Lett. **13**, 5991 (2013).
[9] A. L. Falk, K.-C. Chiu, D. B. Farmer, Q. Cao, J. Tersoff, Y.-H. Lee, P. Avouris, and S.-J. Han, Phys. Rev. Lett. **118**, 257401 (2017).
[10] M. V. Shuba, G. Y. Slepyan, S. A. Maksimenko, C. Thomsen, and A. Lakhtakia, Phys. Rev. B **79**, 155403 (2009).
[11] T. Morimoto and T. Okazaki, Appl. Phys. Express **8**, 055101 (2015).
[12] A. Ugawa, A. G. Rinzler, and D. B. Tanner, Phys. Rev. B **60**, R11305(R) (1999).

[13] F. Borondics, K. Kamaras, M. Nikolou, D. B. Tanner, Z. H. Chen, and A. G. Rinzler, Phys. Rev. B **74**, 045431 (2006).
[14] M. V. Shuba, A. G. Paddubskaya, P. P. Kuzhir, S. A. Maksimenko, G. Valusis, N. A. Poklonski, S. Bellucci, G. Kenanakis, and M. Kafesaki, J. Appl. Phys. **119**, 104303 (2016).
[15] S. Reich, C. Thomsen, and J. Maultzsch, *Carbon Nanotubes: Basic Concepts and Physical Properties* (Wiley-VCH, Berlin, 2004).
[16] M. V. Shuba, S. A. Maksimenko, and A. Lakhtakia, Phys. Rev. B **76**, 155407 (2007).
[17] F. Wang, M. E. Itkis, and R. C. Haddon, Nano Lett. **10**, 937 (2010).
[18] D. L. Carroll, P. Redlich, X. Blase, J.-C. Charlier, S. Curran, P. M. Ajayan, S. Roth, and M. Rühle, Phys. Rev. Lett. **81**, 2332 (1998).
[19] M. U. Kahaly, J. Appl. Phys. **105**, 024312 (2009).
[20] V. Barone, J. E. Peralta, J. Uddin, and G. E. Scuseria, J. Chem. Phys. **124**, 024709 (2006).
[21] T. Koretsune and S. Saito, Phys. Rev. B **77**, 165417 (2008).
[22] L. Panchakarla, A. Govindaraj, and C. Rao, Inorganica Chimica Acta **363**, 4163 (2010).
[23] D. Jana, C.-L. Sun, L.-C. Chen, and K.-H. Chen, Prog. Mater. Sci. **58**, 565 (2013).
[24] L. H. Chan, K. H. Hong, D. Q. Xiao, T. C. Lin, S. H. Lai, W. J. Hsieh, and H. C. Shih, Phys. Rev. B **70**, 125408 (2004).
[25] M. A. Kanygin, O. V. Sedelnikova, I. P. Asanov, L. G. Bulusheva, A. V. Okotrub, P. P. Kuzhir, A. O. Plyushch, S. A. Maksimenko, K. N. Lapko, A. A. Sokol, O. A. Ivashkevich, and P. Lambin, J. Appl. Phys. **113**, 144315 (2013).
[26] S. M. Vieira, O. Stphan, and D. L. Carroll, J. Mater. Res. **21**, 3058 (2006).
[27] A. O. Plyushch, A. A. Sokol, K. N. Lapko, P. P. Kuzhir, Y. V. Fedoseeva, A. I. Romanenko, O. B. Anikeeva, L. G. Bulusheva, and A. V. Okotrub, Phys. Solid State **56**, 2537 (2014).
[28] A. Okotrub, Y. Shevtsov, L. Nasonova, D. Sinyakov, L. Mazalov, A. Chuvilin, and A. Gutakovskij, Inorg. Mater. **32**, 974 (1996).
[29] A. Okotrub, L. Bulusheva, A. Romanenko, A. Chuvilin, N. Rudina, Y. Shubin, N. Yudanov, and A. Gusel'nikov, Appl. Phys. A **72**, 481 (2001).
[30] F. Hennrich, S. Lebedkin, S. Malik, J. Tracy, M. Barczewski, H. Rosner, and M. Kappes, Phys. Chem. Chem. Phys. **4**, 2273 (2002).
[31] M. V. Shuba, A. G. Paddubskaya, P. P. Kuzhir, S. A. Maksimenko, E. Flahaut, V. Fierro, A. Celzard, and G. Valusis, J. Phys. D: Appl. Phys. **50**, 08LT01 (2017).
[32] G. G. Fuentes, E. Borowiak-Palen, M. Knupfer, T. Pichler, J. Fink, L. Wirtz, and A. Rubio, Phys. Rev. B **69**, 245403 (2004).
[33] S. Bao, J. Zheng, G. Yang, and J. Chen, Physica B: Condensed Matter **404**, 4090 (2009).
[34] H.-Y. Chiu, V. V. Deshpande, H. W. C. Postma, C. N. Lau, C. Mikó, L. Forró, and M. Bockrath, Phys. Rev. Lett. **95**, 226101 (2005).
[35] M. V. Shuba, A. V. Melnikov, A. G. Paddubskaya, P. P. Kuzhir, S. A. Maksimenko, and C. Thomsen, Phys. Rev. B **88**, 045436 (2013).
[36] G. Y. Slepyan, M. V. Shuba, S. A. Maksimenko, C. Thomsen, and A. Lakhtakia, Phys. Rev. B **81**, 205423 (2010).
[37] M. F. Lin and K. W.-K. Shung, Phys. Rev. B **50**, 17744 (1994).